

# Techno-economic feasibility study of a solar-powered distributed cogeneration system producing power and distillate water: Sensitivity and exergy analysis

Diederik Coppitters<sup>a,b,c,\*</sup>, Francesco Contino<sup>a,b</sup>, Ahmed El-Baz<sup>d</sup>, Peter Breuhaus<sup>e</sup>, Ward De Paepe<sup>c</sup>

<sup>a</sup>*Fluid and Thermal Dynamics (FLOW), Vrije Universiteit Brussel, Pleinlaan 2, 1050 Brussels, Belgium*

<sup>b</sup>*Combustion and Robust Optimization Group (BURN), Vrije Universiteit Brussel (VUB) and Université Libre de Bruxelles (ULB), 1050 Brussels, Belgium*

<sup>c</sup>*Thermal Engineering and Combustion Unit, University of Mons (UMONS), Place du parc 20, 7000 Mons, Belgium*

<sup>d</sup>*Department of Mechanical Engineering, Faculty of Engineering, The British University in Egypt, Cairo 11837, Egypt*

<sup>e</sup>*Department of Energy, International Research Institute of Stavanger, Professor Olav Hanssens vei 15, 4021 Stavanger, Norway*

---

## Abstract

To satisfy the increasing demand for energy and potable water, large-scale cogeneration is widely integrated. However, in remote locations, the lack of power system infrastructure limits the integration of large-scale systems. Consequently, a large portion of inhabitants has no access to electricity and the pressure on groundwater resources increases drastically. To address this power and water scarcity, a distributed cogeneration system consisting of a solar-powered micro Gas Turbine and desalination system is considered. Since the integration of solar energy in distributed cogeneration systems is uncertain, we performed a feasibility study. This paper covers the modelling, sensitivity and exergy analysis and 3 desalination systems designs, each making a trade-off between smaller plant size and higher performance. Introducing solar energy in the micro gas turbine results in an increase in electrical efficiency by 3.2% absolute. The proposed designs achieve a levelized cost of water between 1.78 \$/(m<sup>3</sup>/d) and 1.92 \$/(m<sup>3</sup>/d), which is comparable with conventional solar-powered desalina-

---

\*Corresponding author

Email address: [dcoppitt@vub.be](mailto:dcoppitt@vub.be) (Diederik Coppitters)

### Nomenclature

BF	Brine Flash	PR	Performance Ratio
CAPEX	Capital expenditure, \$	$\dot{Q}_{CC}$	heat in combustion chamber, W
CC	Combustion Chamber	RC	Radial Compressor
CRF	Capital Recovery Factor	STR	Solar Tube Receiver
DCS	Distributed Cogeneration System	$T$	temperature, °C
DF	Distillate Flash	TBT	Top Brine Temperature, °C
DSH	DeSuperHeater	TIT	Turbine Inlet Temperature, °C
DVC	Dual Vane Compressor	$\dot{V}_w$	distillate water production, m <sup>3</sup> /d
FWH	Feed Water Heater	$\dot{W}_{RC}$	power output radial compressor, W
HRSG	Heat Recovery Steam Generator	$\dot{W}_{turb}$	power output turbine, W
$i$	effective interest rate	$\dot{X}$	exergy, kW
$\dot{m}$	mass flow rate, kg/s	$\Delta T$	temperature difference per effect, °C
MED-TVC	Multi-Effect Distillation with Thermal Vapour Compression	$\eta_{el}$	electrical efficiency
mGT	micro Gas Turbine		
$n$	lifetime, year		
OPEX	Operational expenditure, \$		

tion plants. Therefore, these designs demonstrate the feasibility of integrating solar energy in distributed cogeneration systems and provide a promising solution towards cost-efficient, renewable-based power and water cogeneration in remote locations. The future work will enhance the economic analysis by including an intermittent solar energy supply.

*Keywords:* Distributed cogeneration, levelized cost of water, micro gas turbine, multi-effect distillation with thermal vapour compression, sensitivity and exergy analysis.

## 1. Introduction

Despite the immense potential of solar energy in Africa, the lack of power grid infrastructures and the low national incomes of most African countries constrain the integration of bulk power generation systems, leading to 1 out of 3 inhabitants without access to electricity [1, 2]. Next to the absence of electricity in remote African areas, the local potable water demand increases rapidly, as a result of the continuous population growth. To comply with this increasing water demand, local governments increase pressure on their groundwater resources, which eventually leads to early groundwater depletion [3]. To address the dual demand of electricity and potable water, a widely integrated solution is the cogeneration of power and water (conversion of sea water into potable water) [4–7]. However, such systems are generally constructed on a larger scale, producing power  $\approx 10^2$  MW and water  $\approx 10^4$  m<sup>3</sup>/d, which is not suitable for remote African areas. Instead, Distributed Cogeneration Systems (DCS) (e.g. small-scale production of power, heat, potable water) provide an alternative solution.

In the framework of small-scale heat and power cogeneration, micro Gas Turbines (mGT) and reciprocating engines receive particular interest [8–12]. The exhaust heat of mGTs is high-grade, which makes it a suitable heat source for industrial applications. Moreover, the low vibration level and low maintenance cost, due to the absence of reciprocating components, are significant advantages of the mGT [12]. The integration of solar energy in mGTs is investigated as well. Lanchi et al. coupled concentrated solar power with an mGT, by replacing the boiler by a solar dish [13]. Since high-grade waste heat is still available at the turbine stack, a desalination unit can be coupled with the mGT, resulting in a small-scale water and power cogeneration system.

Desalination processes are divided into three main groups: Membrane, thermal and chemical technologies [14]. The chemical approach is not suitable for managing sea water, due to the high amount of dissolved solids [14]. A typical membrane desalination technology is Reverse Osmosis (RO), which dominates

the global desalination technology market by over 60% [15]. This distribution is not uniform for every country, as the choice of the most appropriate desalination process highly depends on the region. In the United States of America, Spain and Japan, RO is the most widespread [16]. In the Middle East, thermal processes are more common, due to their smooth integration in power plants and their proven high operational reliability, even at high sea water salinity and temperature [17]. In the Arab states of the Persian Gulf, 70% of the installed desalination plants are based on thermal processes [17]. In Italy and the Caribbean Islands, the technology distribution is more balanced [16]. Despite RO is the most efficient desalination technology, a high salinity increases the pump pressure significantly and the handling of high-temperature sea water requires expensive membranes [14, 18]. Moreover, the otherwise wasted heat in the exhaust gas of the mGT implies the use of a thermal desalination process, as opposed to membrane-based desalination. Two thermal desalination processes are generally used: Multi-Effect Distillation with Thermal Vapour Compression (MED-TVC) and Multi-Stage Flash distillation (MSF). Since MED(-TVC) plants achieve higher energy efficiencies than MSF plants [17, 19, 20], a MED-TVC system is coupled with the mGT to convert sea water into distillate water by using waste heat from the turbine stack.

Despite the abundantly available literature on large-scale electric power and water production cogeneration systems, research on small-scale desalination systems is limited [21, 22]. Moreover, the integration of solar energy in DCS used for power and distillate water generation is still uncertain, as solar-based hybrid systems are still in a research stage, coupling solar hybrid mGTs with desalination plants is not yet evaluated in depth and no prototypes currently exist. Therefore, the main novelty and contribution of the authors is the conduction of a techno-economic feasibility study of integrating solar energy in a novel DCS, producing power and potable water. The DCS consists of a mGT, extended with a Solar Tube Receiver (STR) and solar-powered Dual Vane Compressor (DVC), and a MED-TVC system coupled with the turbine stack. The DVC and STR are included to compress and preheat part of the air. This novel mGT cy-

cle ensures a continuous heat and power supply, as opposed to design where the combustor is replaced by a solar receiver. A design point of the solar-powered mGT cycle, based on the Turbec T100 mGT specifications, is evaluated. Thereafter, the MED-TVC goes through a feasibility study, to validate the feasibility of the DCS. When proven feasible, the DCS can prevent early groundwater resource depletion and can comply with the potable water and power demand in remote Africa. This paper covers the modelling of the solar-powered mGT cycle and the MED-TVC desalination plant in section 2. The gain in electrical efficiency of the renewable-powered mGT, the sensitivity and exergy analysis of the MED-TVC system and the final designs are described in section 3, followed by the conclusions in section 4.

## **2. Distributed Cogeneration System (DCS) description and modelling**

The Distributed Cogeneration Plant (DCS) consists of a solar-powered mGT cycle, operating as a Combined Heat and Power unit, coupled with a MED-TVC desalination plant. This section provides the solar-powered mGT and MED-TVC plant description and their modelling and concludes with the MED-TVC model validation.

### *2.1. Solar-powered micro Gas Turbine (mGT) cycle*

To generate electricity and heat, a solar-powered mGT cycle for the DCS is considered (Figure 1). A part of the total air stream in the mGT is compressed in the solar-powered (i.e. power from a photovoltaic system) Dual Vane Compressor (DVC) and preheated in the Solar Tube Receiver (STR). Afterwards, it mixes with the air compressed in the Radial Compressor (RC). The total air flow reaches the Turbine Inlet Temperature (TIT) in the Combustion Chamber (CC) by burning fuel, whereafter it expands over the turbine (Turb). This expansion in the turbine generates mechanical power to drive the RC and a high-speed generator, while waste heat becomes available at the turbine outlet.

To quantify the mechanical power and exhaust heat of the turbine, each component of the cycle is integrated and connected in an Aspen Plus simulation model. The parameters of the traditional Brayton cycle, being the RC, CC and turbine, are based on the Turbec T100 mGT [23]. The RC operation is simulated using a compressor map [24]. This compressor produces a discharge pressure of approximately 4 bar, while the discharge pressure of the DVC is slightly higher to compensate the pressure losses in the STR. For the DVC, a novel design of a sliding-vane rotary compressor is selected. The two-stage novelty elevates the pressure ratio, while higher volumetric efficiencies and higher continuity of flow is achieved, as opposed to other positive displacement air compressors [25]. The novel DVC is defined with a polytropic design efficiency and a mechanical efficiency of 79 % and 90 % respectively. Assuming that the polytropic efficiency changes little around the design point, both efficiencies are considered constant. To simulate the air preheating after compression in the DVC, the STR is modelled based on the design presented by Amsbeck et al. [26]. The operating conditions of the CC and turbine are extracted from an experimentally-validated model of the Turbec T100 mGT [27]: In the CC, a pressure loss of 5 %, a combustion efficiency of 100 % and a 10 kW heat loss to the environment is assumed [23], while the turbine operates at an isentropic efficiency of 85 %, a choking constant of 6.5 and a 40 mbar back pressure [23, 28]. Additionally, the STR is validated using [26], making a full model experimental validation not necessary. To quantify the mGT performance, the electrical efficiency  $\eta_{el}$  of the mGT is defined as:

$$\eta_{el} = \frac{\dot{W}_{turb} - \dot{W}_{RC}}{\dot{Q}_{CC}}. \quad (1)$$

## 2.2. *Multi-Effect Distillation with Thermal Vapour Compression (MED-TVC) plant*

To recuperate the waste heat from the turbine stack, a Multi-Effect Distillation with Thermal Vapour Compression (MED-TVC) system is considered. In

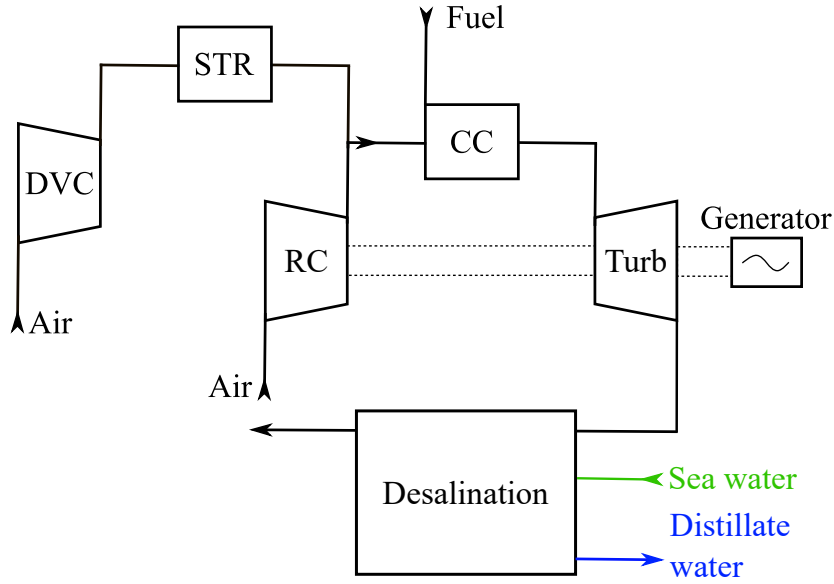


Figure 1: A schematic overview of the considered Distributed Cogeneration System (DCS) is presented. In this DCS, the solar-powered Dual Vane Compressor (DVC) and Solar Tube Receiver (STR) compress and preheat part of the air stream. This air stream mixes with the compressed air coming from the Radial Compressor (RC). The resulting mixture is heated in the Combustion Chamber (CC) up to the Turbine Inlet Temperature (TIT). In the turbine (Turb), the air mixture expands, resulting in mechanical power and waste heat at the outlet. To recover the waste heat, a Heat Recovery Steam Generator (HRSG) uses the heat to produce steam. The steam is used as a heat source in the thermal desalination system to convert sea water into distillate water.

this section, the system operation is described, followed by the system modelling and validation.

### 2.2.1. MED-TVC system description

A typical 4-stage MED-TVC plant with Heat Recovery Steam Generator (HRSG) is presented in Figure 2. The steam ejector extracts steam from the fourth effect and mixes that steam with the stream coming from the HRSG. In the steam ejector, the pressure of the superheated steam mixture increases by Thermal Vapour Compression (TVC) and reaches a saturated state by mixing

with liquid water in the DeSuperHeater (DSH). Thereafter, the saturated steam is used as a heat source in the first effect to partially evaporate the incoming feed water. In the tubes of the first effect, the steam condenses and the resulting latent heat is transferred to the sprayed sea water, which leads to partial evaporation of the sea water. As the sea water partly evaporates, the remaining salt mixes with the untouched sea water, resulting in brine water with increased salinity. The produced water vapour is (ideally) free of salt and is transferred through the Feed Water Heater (FWH) to preheat the incoming feed water. Thereafter, the steam enters the next effect where the process repeats itself. The condensed salt-free water coming from each effect flows through external flash boxes (DF). In these flash boxes, water vapour is formed due to flash evaporation, resulting in an increased steam mass flow rate in the effect following the flash box. After the fourth effect, part of the steam is used in the steam ejector, while the remaining fraction enters the condenser (COND), where the steam condenses to preheat the sea water. Depending on the desired mass flow rate of the feed water distributed over the effects, part of the preheated sea water is discarded [29].

### *2.2.2. MED-TVC system modelling*

To simplify the simulation with a negligible loss in accuracy, a number of typical assumptions are implemented [18, 29, 30]:

- The feed water is equally distributed over the effects;
- The temperature difference across each effect is the same and equal to the liquid temperature difference in each FWH;
- The heat loss from the effects to the environment is negligible;
- The produced vapour is salt-free;
- The pressure and temperature losses in the connecting tubes are neglected.

The steam, necessary in the desalination process, is produced in a HRSG using the high-grade waste heat from the mGT. The main components of a single

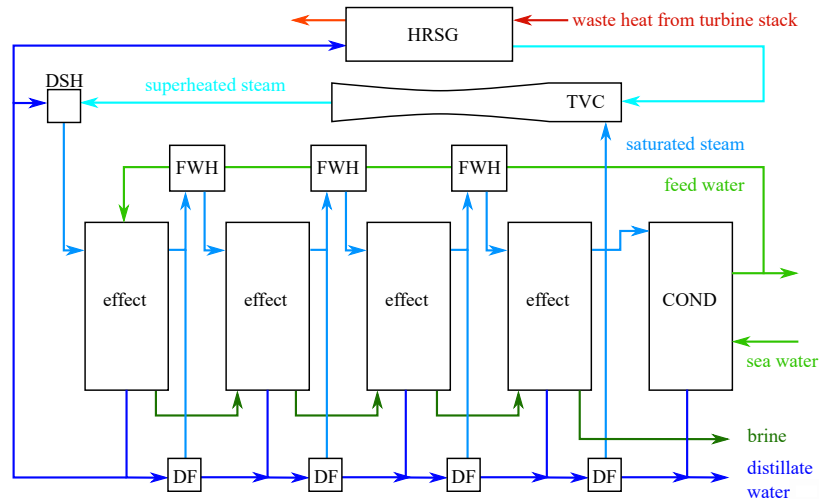


Figure 2: This schematic overview of a Multi-Effect Distillation plant using Thermal Vapour Compression (MED-TVC) illustrates that steam is recycled from the last effect and compressed in a steam ejector, after mixing with high-pressure steam from the Heat Recovery Steam Generator (HRSG). The accumulated steam is used in the effects as a heat source to convert sea water into distillate water.

pressure HRSG are an economizer, evaporator and superheater. The economizer heats up the liquid close to the saturated state, whereupon it is vaporized in the evaporator and reaches a superheated state in the superheater. To restrain the exergy destruction in the HRSG, the pinch point, which is defined as the difference between the gas temperature at the evaporator entry and the water saturation temperature, should be as low as possible [31]. As the cost of the HRSG increases exponentially when the pinch point temperature reaches zero, a minimal offset is defined between  $5^{\circ}\text{C}$  and  $15^{\circ}\text{C}$  [32]. In the Aspen Plus simulation model, the HRSG is modelled by connecting 3 heat exchanger blocks, representing respectively the economizer, evaporator and superheater.

After being produced in the HRSG, the high-pressure steam enters the steam ejector. The steam mixes with low-pressure steam extracted from the last effect, resulting in intermediate pressure steam at the ejector outlet. The intermediate steam pressure that is achieved by the steam ejector is an important design parameter, as it corresponds to the steam saturation pressure in the first ef-

fect. Therefore, the steam ejector should be properly designed. The steam ejector design is aimed to optimize the compression ratio, which is defined as the discharged-to-entrained (intermediate-to-low) steam pressure ratio. The compression ratio depends on the expansion ratio and entrainment ratio, which are defined as the motive-to-entrained (high-to-low) steam pressure ratio and motive-to-entrained steam mass flow rate ratio, respectively. The relation between these performance parameters and the motive steam pressure upper limit are based on published data of existing steam ejectors [33, 34]. The compression ratio is limited between 1.81 and 4, while the entrainment ratio cannot exceed 4 [35]. In the Aspen Plus model, the steam ejector is represented by an adiabatic mixer and operates according to the model described by Hassan et al. [33].

After the steam leaves the steam ejector and reaches a saturated state in the DSH, the steam enters the first effect. In this first effect, the steam operates as a heat source, used to partially evaporate the sea water. To model the characteristic of a single effect in Aspen Plus, the method proposed by Zak et al. is considered [18] (Figure 3). In the model represented in Figure 3, the steam produced in effect  $n - 1$  enters the consecutive effect  $n$ , where it condenses. The latent heat released during condensation is used to partially evaporate the incoming feed water (feed water,  $n$ ). The condensation and resulting evaporation is modelled in Aspen Plus by combining a heater block (HEAT) and a flash evaporator block (EVAP), where the heat duty from the condensing process  $\dot{Q}$  in the heater is transferred to the evaporator. In the evaporator, the feed water partly evaporates, resulting in water vapour (vapour,  $n$ ) and brine (brine,  $n$ ).

The brine from the previous effect (brine,  $n - 1$ ) accumulates with the remaining brine in effect  $n$ , resulting in accumulated brine that is sent to the next effect in line (brine,  $n + 1$ ). Since the operating pressure in each consecutive effect is lower than the previous, the incoming brine undergoes minor flash evaporation, resulting in an increase in the produced steam mass flow rate (vapour,  $n$ ). To represent this consecutive pressure reduction in the model, a flash evaporator (BF) is integrated. Similar to the brine flash evaporation, flash boxes are integrated into the system to perform a flash evaporation on the produced

distillate water (DF), to further increase the produced steam mass flow rate. The total accumulated steam is sent through a FWH, modelled with a heat exchanger block, to preheat the incoming feed water (feed water,  $n + 1$ ).

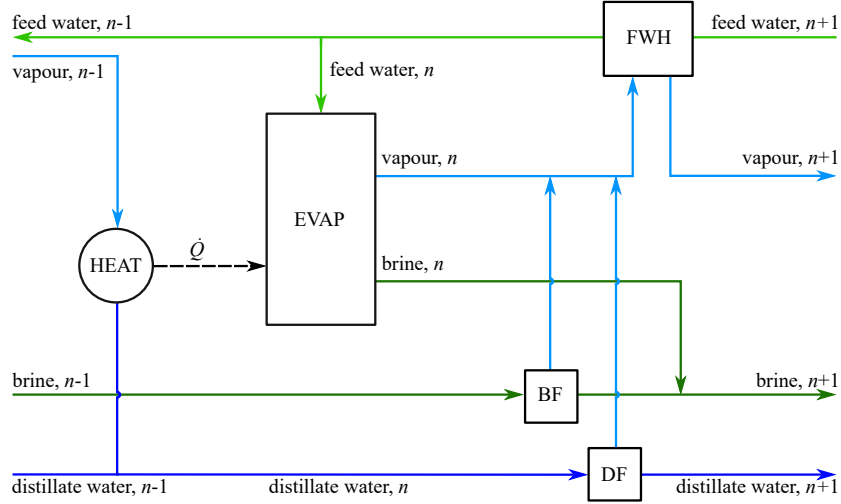


Figure 3: The schematic representation of a single effect of a MED-TVC system reveals that the heat extracted in the condenser (HEAT) is used to partly evaporate the feed water in the evaporator (EVAP). The resulting vapour preheats the incoming feed water in the Feed Water Heater (FWH). Figure adapted from [18].

To increase the total distillate water mass flow rate produced by the MED-TVC system, a string of operating effects is created, where each consecutive effect operates at a reduced pressure (and reduced saturation temperature). To keep the operating costs low, the upper limit for the temperature difference between each effect  $\Delta T$  is set at  $5^\circ\text{C}$  [35]. The temperature difference between each effect is proportional to the heat driving force (i.e. the temperature difference between the incoming steam and the saturation temperature in the effect). Increasing this driving force results in a decrease in heat transfer area of the effect. Consequently, a high total temperature difference is beneficial (i.e. the difference between the saturation temperature in the first and last effect). Despite a high evaporation temperature in the first effect (i.e. Top Brine Temperature (TBT)) is beneficial for the total temperature difference, a high TBT induces salt-scaling on the tubes in the first effect, resulting in corrosion and a

decrease in heat transfer area [36]. To avoid this phenomenon, the TBT upper limit is typically set at 70 °C [36–38]. Next to maximizing the TBT, the second option to maximize the total temperature difference is to reduce the evaporation temperature in the last effect. The lower limit of this evaporation temperature is however constrained by the incoming feed water temperature. To avoid early feed water evaporation before entering the effect, the evaporation temperature in each effect is fixed at least 2 °C above the feed water temperature [35]. Moreover, the feed water is preheated in the condenser, which further increases the lower evaporation temperature limit in the last effect. Consequently, a small temperature increase of the sea water in the condenser is preferable over a larger temperature increase. However, reducing the temperature difference induces an increase in the sea water mass flow rate intake in the condenser, in order to fully condense the vapour. In our application, similar to [35], a sea water temperature increase of 10 °C in the condenser is assumed. The sea water temperature and salinity are set at 28.4 °C and 42 000 ppm respectively, based on the characteristics of the Red Sea [39, 40].

The ELECNRTL physical property method is selected to evaluate the Aspen Plus model. ELECNRTL comprises both aqueous and aqueous/organic electrolyte systems over the whole range of electrolyte concentrations. The vapour phase properties are calculated using the Redlich-Kwong equation of state [41].

### 2.2.3. Economic evaluation

To determine the economic performance of the MED-TVC, the Levelized Cost Of Water (LCOW) is quantified as [20]:

$$\text{LCOW} = \frac{\text{CRF} \cdot \text{CAPEX} + \text{OPEX}}{\dot{V}_w}, \quad (2)$$

where the Capital Recovery Factor (CRF) is defined as [20]:

$$\text{CRF} = \frac{i(1+i)^n}{(1+i)^n - 1}. \quad (3)$$

A lifetime  $n$  of 25 years and an effective interest rate  $i$  of 6 % is selected [20]. The effective interest rate is considered with annual compounding and the cor-

rection by the expected inflation rate and the risk factor of the owners is assumed. The CAPEX includes the direct and indirect capital costs, such as the main investment, post-treatment, open sea water intake and water storage costs. The OPEX comprises the electricity costs, spare parts replacement, labour cost and insurance. The cost of the heat source is neglected in this analysis, as it is considered a waste product of the mGT. The specific CAPEX and OPEX of a MED-TVC system producing 9000 m<sup>3</sup>/d are defined at 3064 \$/(m<sup>3</sup>/d) and 177 \$/(m<sup>3</sup>/d) respectively [20]. Nevertheless, as the economies of scale apply, it is reasonable to consider that large-scale MED-TVC systems achieve a reduced specific cost compared to small-scale systems. Therefore, a scale effect on the specific CAPEX is considered [20]:

$$\frac{\text{CAPEX}_{\text{large}}}{\text{CAPEX}_{\text{small}}} = \left( \frac{\dot{V}_{\text{w,large}}}{\dot{V}_{\text{w,small}}} \right)^{\alpha}, \quad (4)$$

where the scaling factor  $\alpha$  is quantified as 0.82 for MED-TVC systems [20].

#### 2.2.4. Model validation

Our MED-TVC model, constructed in Aspen Plus, is validated using several models from literature [18, 42], which have been validated with experimental data. Input data from literature is incorporated in the simulation model and the results are compared with the results from literature (Table 1). First, a 12-effect MED-TVC plant with FWH is simulated with our Aspen Plus model and the results are compared with the results from Zak et al. [18]. As expected, there is a little deviation between the Aspen Plus model and the reference model (maximum 0.9%). The small deviation is due to the rounded variables in the work and the uncertainty on the recovery ratio. A second model, which comprises 9 effects, is built based on the model of Luo et al. [42]. In this model, the entrained steam is subtracted from an intermediate effect (effect 5 out of 9). Therefore, not all effects are fed by an equal amount of feed water, leading to a deviation of the performance results (maximum 1.2%). In conclusion, the results correspond well to the results of the reference papers, resulting in a validated MED-TVC model.

Table 1: The Aspen Plus model results correspond well to the results of the reference models.

Parameter	Ref. [18]	Aspen Plus	Ref. [42]	Aspen Plus
<b>Inputs</b>				
Number of effects	12	12	9	9
Temperature difference/effect $\Delta T$ , °C	1.81	1.81	3.8	3.8
Salinity feed water, ppm	46 000	46 000	35 000	35 000
Motive steam pressure, bar	0.312	0.312	3.61	3.61
<b>Aspen Plus simulation results</b>				
Brine temperature, °C	42.5	42.1	35.1	35.0
Top Brine Temperature TBT, °C	62	62	65.6	65.6
<b>Performance parameters</b>				
Performance ratio PR	17.2	17.2	11.3	11.2
Entrainment ratio	2.42	2.42	1.87	1.87
Salinity brine, ppm	72 000	72 082	186 000	184 515

### 3. Results and discussion

After the modelling of the DCS, the quantities of interest are quantified to determine the system performance. First, the exhaust heat exergy at the turbine outlet is quantified. This corresponds to the heat source for the desalination plant and is therefore the starting parameter for the MED-TVC design. After a parametric sensitivity analysis, 3 MED-TVC designs are proposed, each one of them making a trade-off between minimum plant size and maximum distillate water production.

#### 3.1. Solar-powered mGT cycle

In order to define the generated electric power and the waste heat of the turbine, the mGT model is simulated in Aspen Plus (Figure 4) with a reference state that corresponds to the air inlet conditions (25 °C and 1.013 bar). The generator provides 123.3 kW, while the solar-powered DVC covers 18.1 kW. The

exhaust gas stream at the turbine outlet has a temperature of 670 °C, while still 242.3 kJ/s of exergy is available for the MED-TVC plant to convert sea water into distillate water.

Assuming a constant, sufficient solar energy supply to run the DVC and STR, the electrical efficiency of the mGT cycle is 20.8 %. In comparison, operating without the DVC and STR reduces the electrical efficiency to 17.6 %, which corresponds to the electrical efficiency of micro gas turbines without recuperator, ranging between 16 % and 20 % [43]. Consequently, introducing the DVC and STR in the mGT cycle increases the electrical efficiency by 3.2 % absolute.

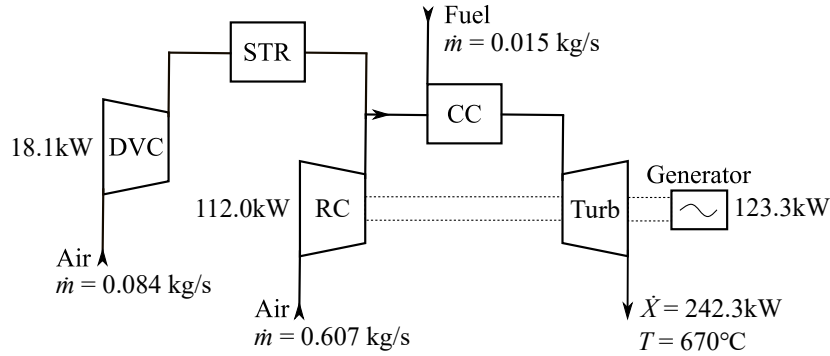


Figure 4: The energy and exergy analysis of the solar-powered micro Gas Turbine (mGT) cycle reveals that the net mechanical power generated by the turbine is 123.3 kW, which will be converted by the generator into electrical power. At the turbine outlet, 242.3 kJ/s of exergy is available.

### 3.2. MED-TVC desalination plant

The MED-TVC desalination plant is powered by the available exergy at the turbine outlet to convert sea water into distillate water. To define the operational parameters of the system, first, a sensitivity analysis is performed. Based on the findings of this sensitivity analysis, 3 different MED-TVC plant designs are suggested for the DCS system. The first design focuses on restraining the heat transfer area, while the second design is an intermediate solution between low heat transfer area and high distillate water production. The final design focuses on optimizing the distillate water production.

### 3.2.1. Sensitivity and exergy analysis

To optimize the amount of distillate water produced by the desalination plant, the exergy destruction in the HRSG, steam ejector and DSH should be minimized. Then, the maximum exergy is available in the effects to induce the conversion of sea water into distillate water. The main parameters are initially identified, followed by a study on their impact on the exergy efficiency of the different MED-TVC components. Thereafter, a sensitivity analysis of the main operating parameters in the effects is performed.

To recover the waste heat from the mGT stack, a HRSG is installed (Figure 2). Through the sensible heat transfer from the air stream to the water flow at the cold inlet, the water increases in temperature and evaporates. To recuperate as much exergy as possible from the air stream in the water flow, the exergy efficiency of the HRSG is studied. The pressure of the produced steam in the HRSG (i.e. motive steam) significantly influences the exergy efficiency of the HRSG (Figure 5). Increasing the motive steam pressure is clearly beneficial for the exergy efficiency, as it increases the water saturation temperature and therefore decreases the exergy destruction in the HRSG [31].

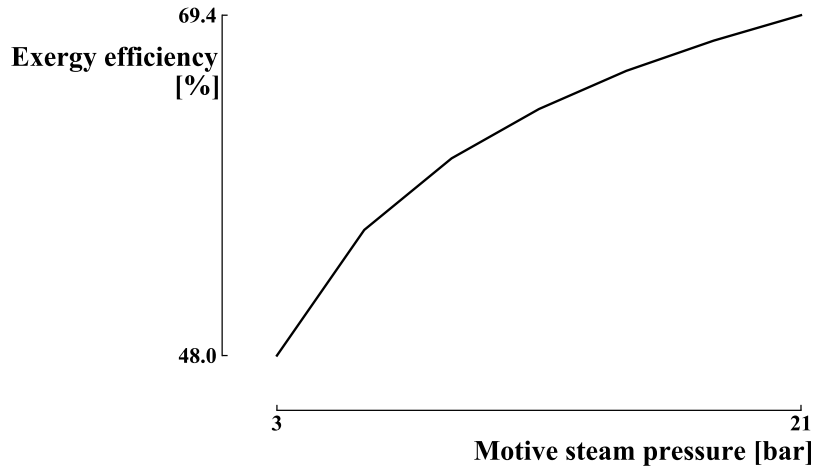


Figure 5: Presenting the exergy efficiency as a function of the motive steam pressure indicates that increasing the motive steam pressure improves the exergy efficiency of the Heat Recovery Steam Generator (HRSG), due to the increase in steam saturation temperature.

After the HRSG, exergy destruction occurs in the steam ejector and DSH before the exergy becomes available for desalination in the effects. As expected, the exergy is mostly destroyed in the TVC (Figure 6), since a large temperature drop (from 215 °C to  $\approx 70$  °C) and pressure drop (from 21 bar to  $\approx 0.3$  bar) occur between the steam at the HRSG outlet and steam ejector outlet. In comparison, a relatively small amount is destroyed in the DSH, since only the remaining sensible heat is lost in the DSH. To achieve the highest exergy at the outlet of the DSH, the motive steam pressure has to be selected at its upper limit (i.e. 21 bar). This amount of exergy at the DSH outlet corresponds to the exergy available for the sea water evaporation process in the first effect.

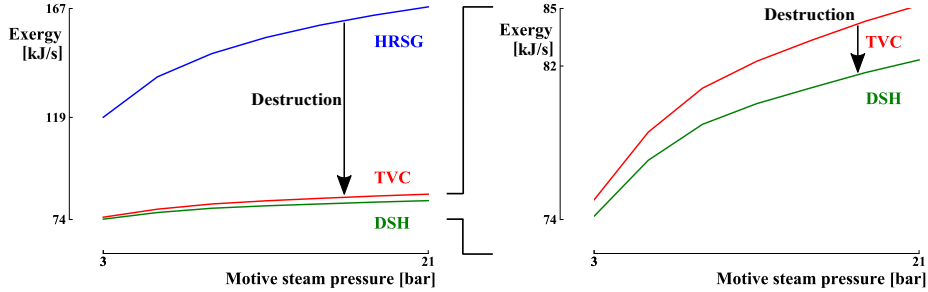


Figure 6: The exergy destruction in the Heat Recovery Steam Generator (HRSG), during Thermal Vapour Compression (TVC) and in the DeSuperHeater (DSH) is presented in function of the motive steam pressure. Clearly, selecting the motive steam pressure upper limit value results in the highest exergy available to power the sea water evaporation process.

To optimize the conversion from sea water into distillate water, the operating parameters of the effects and steam ejector are studied. To quantify the desalination performance, the Performance Ratio (PR) (i.e. distillate-to-motive steam mass flow rate ratio) is analyzed. Despite an optimal PR at minimum feed water mass flow rate, the brine salinity increases drastically in that range (Figure 7). A high salinity leads to high salt-scaling on the effect tubes and increases the overall sea water salinity when disposed back into the sea. Therefore, the brine salinity is usually limited [29]. In the proposed model, a common brine salinity upper limit of 70.000 ppm is selected [37]. To comply with this environmental limit, the minimum feed water mass flow rate is limited. Despite

this lower limit on the feed water mass flow rate limits the PR improvement, the possible gain in PR is relatively small by varying the feed water mass flow rate (Figure 7).

In contrast with the feed water mass flow rate, the PR increases significantly when decreasing the entrainment ratio (Figure 7). On the other hand, decreasing the entrainment ratio results in a decrease of the compression ratio in the steam ejector. As the steam ejector discharge pressure is equal to the inlet steam pressure of the first effect, the corresponding saturation temperature and thermal driving force in that effect depend on the compression ratio. Therefore, the compression ratio in the steam ejector has to be sufficient to ensure that the driving force in the first effect is in the range of the driving force in the other effects. To prevent a decrease of the compression ratio when decreasing the entrainment ratio, the motive steam pressure can be increased (Figure 7). When the entrainment ratio reaches 1.96, the motive steam pressure becomes insufficient to reach the fixed compression ratio of the steam ejector. When the entrainment ratio goes below 1.11, the motive steam pressure is above the upper limit selected for the model. Therefore, the operating range for the entrainment ratio is limited between 1.11 and 1.96.

### *3.2.2. MED-TVC design decisions*

Based on the sensitivity and exergy analysis, 3 designs are proposed in this section. Following the sea water temperature and the assumption on the temperature difference for the sea water in the condenser, the evaporation temperature in the last effect is set at 41 °C. When operating at a constant  $\Delta T$  between each consecutive effect, the number of effects installed is proportional to the TBT. To keep the TBT in the range of modern MED-TVC plants, without drastically lowering the  $\Delta T$  and therefore reducing the heat driving force, the designs consist of 4, 6 and 8 effects respectively. Increasing the number of effects results in a higher distillate flow rate, but increases the overall heat transfer area of the plant. Therefore, a trade-off between lower area (and thus capital cost) and higher performance is performed in each design. The first design focuses

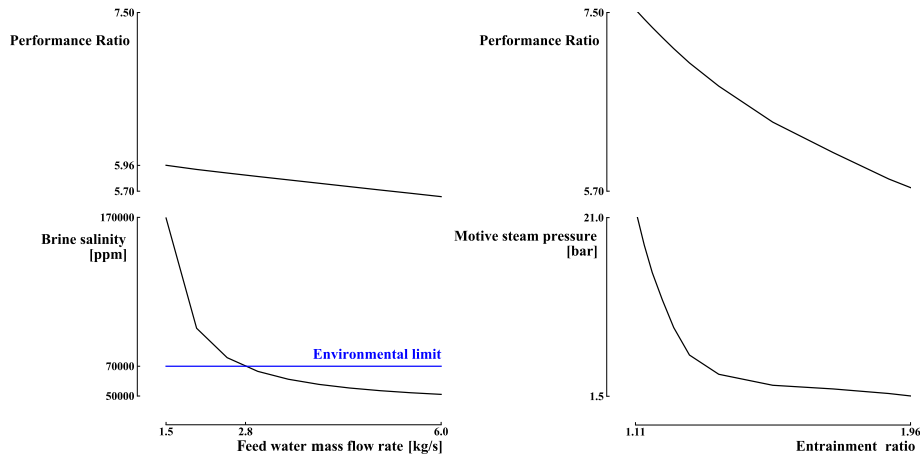


Figure 7: The Performance Ratio (PR) is demonstrated as a function of the feed water mass flow rate and entrainment ratio. Moreover, the effect of the former on the brine salinity and the effect of the latter on the motive steam pressure is presented as well. Reducing the mass flow rate is beneficial for the PR. However, to keep the brine salinity and the driving force acceptable, the lower limit of the feed water mass flow rate is fixed. Decreasing the entrainment ratio improves the PR significantly, but the range of the entrainment ratio is limited due to motive steam pressure limitations.

on restraining the capital cost by minimizing the heat transfer area, the second design is an intermediate solution, while the final design focuses on distillate water production (Table 2).

With 4 effects installed, a maximum temperature drop over the effects of  $5^{\circ}\text{C}$  minimizes the heat transfer area and results in a TBT of  $56^{\circ}\text{C}$ . To keep the thermal driving force in the first effect in the range of the driving force in the other effects, a steam ejector compression ratio of 2.6 is required. Adding 2 more effects to the plant implies a decrease in  $\Delta T$  to curb the TBT. Moreover, a decrease in  $\Delta T$  results in an improved PR, however at the expense of an increase in specific heat transfer area. To achieve a specific heat transfer area in the range of the specific heat transfer area of the 4-effect design, the temperature difference across each effect in this intermediate design is reduced to  $4.2^{\circ}\text{C}$ . This design shows a comparable performance (i.e. similar PR, TBT, specific exergy consumption and specific energy consumption) to the operating MED-

TVC Umm Al-Nar plant in the United Arab Emirates [42]. The final design consists of 8 effects. This design further improves the PR, at the expense of a higher amount of installed effects. The high amount of effects in the plant imposes the temperature difference between the effects to drop further. Next to the clear TBT constraint, which forces the temperature difference to stay below  $4.1^{\circ}\text{C}$ , the steam ejector compression ratio upper limit is violated at a  $\Delta T$  above  $3.6^{\circ}\text{C}$ . At a  $\Delta T$  of  $3.6^{\circ}\text{C}$ , a saturated steam temperature of  $69^{\circ}\text{C}$  is required in the first effect, which corresponds to a discharge pressure of 0.3 bar. This pressure can only be obtained at the steam ejector compression ratio upper limit. Due to this constraint on the temperature difference between each effect, the 8-effect MED-TVC plant specific heat transfer area is clearly higher than for the other designs. When aiming for the same, modern TBT as in the 6-effect design, the temperature difference is set at  $3^{\circ}\text{C}$ , which avoids an excessively high specific heat transfer area and further improves the PR, compared to the other designs.

For the 3 proposed designs, the total investment cost (i.e. including direct and indirect cost) ranges between \$779 000 and \$1 231 000. This result implies that the designs with a higher production rate (i.e. higher PR) are inherently more expensive. Consequently, the 4-effect design delivers the most accessible solution to destitute remote communities, while the other designs provide a solution for more prosperous communities. The resulting LCOW ranges between  $1.78\text{\$/}(\text{m}^3/\text{d})$  and  $1.92\text{\$/}(\text{m}^3/\text{d})$  (Table 2). Consequently, this system achieves a higher LCOW than conventional MED(-TVC) systems (between  $1.21\text{\$/}(\text{m}^3/\text{d})$  and  $1.59\text{\$/}(\text{m}^3/\text{d})$ ), RO systems (between  $1.06\text{\$/}(\text{m}^3/\text{d})$  and  $1.36\text{\$/}(\text{m}^3/\text{d})$ ) and MSF systems (between  $0.84\text{\$/}(\text{m}^3/\text{d})$  and  $1.60\text{\$/}(\text{m}^3/\text{d})$ ) [44]. However, these conventional systems assume a fossil-based energy supply. When comparing with MED(-TVC) systems powered by solar thermal energy (LCOW ranging between  $2.5\text{\$/}(\text{m}^3/\text{d})$  and  $3.0\text{\$/}(\text{m}^3/\text{d})$  [44]), the LCOW of the proposed designs is lower. Therefore, the determined LCOW of the 3 proposed designs provides promising results towards the economic viability of this solar-powered DCS.

Table 2: Design results for the MED-TVC desalination plant.

Parameter	Design 1	Design 2	Design 3
<b>Inputs</b>			
Number of effects	4	6	8
Compression ratio	2.6	3.4	3.2
Temperature difference/effect $\Delta T$ , °C	5.0	4.2	3.0
<b>Aspen Plus simulation results</b>			
Feed water mass flow rate, kg/s	3.368	4.484	5.882
Top Brine Temperature TBT, °C	56.0	62.0	62.0
Distillate water mass flow rate $\dot{V}_w$ , m <sup>3</sup> /d	116.4	154.3	203.1
<b>Performance parameters</b>			
Performance ratio PR	7.4	9.9	13.0
Specific heat transfer area, m <sup>2</sup> /(kg/s)	268.8	269.4	449.2
Entrainment ratio	1.14	1.51	1.42
Specific energy consumption, kJ/kg	351.2	262.3	199.7
Specific exergy consumption, kJ/kg	123.4	92.8	70.7
Total investment cost, k\$	779	983	1231
Levelized Cost Of Water LCOW, \$/m <sup>3</sup>	1.92	1.85	1.78

#### 4. Conclusion

DCS integrated with renewable energy sources provide a viable solution to cover the electricity and distillate water demand in remote locations. As part of the DCS, a typical mGT, extended with a solar heater and a solar-powered compressor, results in a significant fuel consumption reduction, which leads to an increase in electrical efficiency by 3.2% absolute. In addition to the generated electrical power, 242.3 kJ/s of exhaust gas exergy is available at the turbine outlet. By recovering this thermal energy in a MED-TVC desalination plant, sea water can be converted into distillate water. The MED-TVC sensitivity and exergy analysis indicates that varying the feed water mass flow rate allows

regulating the brine salinity and the thermal driving force, while the entrained steam mass flow rate and motive steam pressure are the significant parameters to maximize the distillate water production. Out of these findings, 3 designs of the desalination unit are extracted, each of them making a trade-off between minimum plant size and maximum performance. The 4-effect design delivers an easily accessible solution to remote communities, while the other designs focus on improving the system performance, at the expense of a larger investment cost. The LCOW of the proposed designs ranges between 1.78  $\$/(\text{m}^3/\text{d})$  and 1.92  $\$/(\text{m}^3/\text{d})$ , which is slightly higher than the LCOW of conventional desalination systems, but less expensive than desalination systems powered by solar thermal energy. As a result, these designs not only offer different possibilities to combine a desalination plant with the renewable-powered mGT cycle, but also prove the viability of a DCS integrated with renewable energy sources. Despite the simplified economic approach (i.e. excluding the intermittency of the solar energy), the determined LCOW provides a first indication that this DCS is a promising solution towards cost-efficient, renewable-powered power and water cogeneration in remote locations. To validate this promising indication, future work will focus on a thorough economic analysis of the DCS, including an intermittent solar energy supply.

## 5. Acknowledgements

Funding: The work was supported by ERAfrica [ERAFRICA\_RE-027]. The first author acknowledges the support of Fonds de la Recherche Scientifique - FNRS [33856455-5001419F FRIA-B1].

## References

- [1] A. G. Dagnachew, P. L. Lucas, A. F. Hof, D. E. Gernaat, H.-S. de Boer, D. P. van Vuuren, The role of decentralized systems in providing universal electricity access in Sub-Saharan Africa—A model-based approach, *Energy* 139 (2017) 184–195.

- [2] I. Bugaje, Renewable energy for sustainable development in Africa: a review, *Renewable and sustainable energy reviews* 10 (6) (2006) 603–612.
- [3] F. Trieb, H. Müller-Steinhagen, Concentrating solar power for seawater desalination in the Middle East and North Africa, *Desalination* 220 (1-3) (2008) 165–183.
- [4] W. He, D. Han, L. Xu, C. Yue, W. Pu, Performance investigation of a novel water–power cogeneration plant (WPCP) based on humidification dehumidification (HDH) method, *Energy Conversion and Management* 110 (2016) 184–191.
- [5] L. Wu, Y. Hu, C. Gao, Optimum design of cogeneration for power and desalination to satisfy the demand of water and power, *Desalination* 324 (2013) 111–117.
- [6] A. M. El-Nashar, Cogeneration for power and desalination - state of the art review, *Desalination* 134 (1-3) (2001) 7–28.
- [7] C. Valenzuela, C. Mata-Torres, J. M. Cardemil, R. A. Escobar, CSP+ PV hybrid solar plants for power and water cogeneration in northern Chile, *Solar Energy* 157 (2017) 713–726.
- [8] W. De Paepe, M. Montero Carrero, S. Bram, F. Contino, A. Parente, Waste heat recovery optimization in micro gas turbine applications using advanced humidified gas turbine cycle concepts, *Applied Energy* 207 (2017) 218–229.
- [9] S. Giorgetti, L. Bricteux, A. Parente, J. Blondeau, F. Contino, W. De Paepe, Carbon capture on micro gas turbine cycles: Assessment of the performance on dry and wet operations, *Applied Energy* 207 (2017) 243–253.
- [10] M. Montero Carrero, W. De Paepe, S. Bram, F. Musin, A. Parente, F. Contino, Humidified micro gas turbines for domestic users: An economic and primary energy savings analysis, *Energy* 117 (2016) 429–438.

- [11] M. Montero Carrero, W. De Paepe, A. Parente, F. Contino, T100 mGT converted into mHAT for domestic applications: Economic analysis based on hourly demand, *Applied energy* 164 (2016) 1019–1027.
- [12] P. Pilavachi, Mini-and micro-gas turbines for combined heat and power, *Applied thermal engineering* 22 (18) (2002) 2003–2014.
- [13] M. Lanchi, M. Montecchi, T. Crescenzi, D. Mele, A. Miliozzi, V. Russo, D. Mazzei, M. Misceo, M. Falchetta, R. Mancini, Investigation into the coupling of micro gas turbines with CSP technology: OMSoP project, *Energy Procedia* 69 (2015) 1317–1326.
- [14] T. Younos, K. E. Tulou, Overview of desalination techniques, *Journal of Contemporary Water Research & Education* 132 (1) (2005) 3–10.
- [15] M. Nair, D. Kumar, Water desalination and challenges: the Middle East perspective: a review, *Desalination and Water Treatment* 51 (10-12) (2013) 2030–2040.
- [16] M. Al-Sahali, H. Ettouney, Developments in thermal desalination processes: Design, energy, and costing aspects, *Desalination* 214 (1-3) (2007) 227–240.
- [17] I. S. Al-Mutaz, I. Wazeer, Current status and future directions of MED-TVC desalination technology, *Desalination and Water Treatment* 55 (1) (2015) 1–9.
- [18] G. M. Zak, N. D. Mancini, A. Mitsos, Integration of thermal desalination methods with membrane-based oxy-combustion power cycles, *Desalination* 311 (2013) 137–149.
- [19] S. Ihm, O. Y. Al-Najdi, O. A. Hamed, G. Jun, H. Chung, Energy cost comparison between MSF, MED and SWRO: Case studies for dual purpose plants, *Desalination* 397 (2016) 116–125.
- [20] I. B. Askari, M. Ameri, Techno economic feasibility analysis of Linear Fresnel solar field as thermal source of the MED/TVC desalination system, *Desalination* 394 (2016) 1–17.

- [21] L. Cioccolanti, A. Savoretti, M. Renzi, F. Caresana, G. Comodi, Comparison of different operation modes of a single effect thermal desalination plant using waste heat from m-CHP units, *Applied Thermal Engineering* 100 (2016) 646–657.
- [22] H. C. Duong, P. Cooper, B. Nelemans, T. Y. Cath, L. D. Nghiem, Optimising thermal efficiency of direct contact membrane distillation by brine recycling for small-scale seawater desalination, *Desalination* 374 (2015) 1–9.
- [23] W. De Paepe, F. Contino, F. Delattin, S. Bram, J. De Ruyck, Optimal waste heat recovery in micro gas turbine cycles through liquid water injection, *Applied Thermal Engineering* 70 (1) (2014) 846–856.
- [24] W. De Paepe, M. Renzi, M. Montero Carrero, C. Caligiuri, F. Contino, Micro Gas Turbine Cycle Humidification for Increased Flexibility: Numerical and Experimental Validation of Different Steam Injection Models, *Journal of Engineering for Gas Turbines and Power* 141 (2) (2019) 021009.
- [25] A. Shouman, A. E. D. Hussin, A. Hamed, M. S. El Din, N. Mahmoud, A. El Baz, Performance evaluation of a novel dual vane rotary compressor, in: *IOP Conference Series: Materials Science and Engineering*, Vol. 232, IOP Publishing, 2017, p. 012060.
- [26] L. Amsbeck, R. Buck, P. Heller, J. Jedamski, R. Uhlig, Development of a tube receiver for a solar-hybrid microturbine system, in: *Proceedings of 14th SolarPACES Conference*, Las Vegas, NV, March, 2008, pp. 4–7.
- [27] W. De Paepe, M. Montero Carrero, S. Giorgetti, A. Parente, S. Bram, F. Contino, Exhaust gas recirculation on humidified flexible micro gas turbines for carbon capture applications, in: *ASME Turbo Expo 2016: Turbomachinery Technical Conference and Exposition*, American Society of Mechanical Engineers, 2016, pp. 1–11, GT2016–57265.
- [28] W. De Paepe, F. Delattin, S. Bram, J. De Ruyck, Steam injection experi-

- ments in a microturbine—A thermodynamic performance analysis, *Applied Energy* 97 (2012) 569–576.
- [29] M. Hosseini, I. Dincer, P. Ahmadi, H. B. Avval, M. Ziaasharhagh, Thermodynamic modelling of an integrated solid oxide fuel cell and micro gas turbine system for desalination purposes, *International Journal of Energy Research* 37 (5) (2013) 426–434.
- [30] F. Alasfour, M. Darwish, A. B. Amer, Thermal analysis of METVC + MEE desalination systems, *Desalination* 174 (1) (2005) 39–61.
- [31] M. Gleinser, C. Wieland, The misselhorn cycle: batch-evaporation process for efficient low-temperature waste heat recovery, *Energies* 9 (5) (2016) 337.
- [32] H. C. Reuter, S. A. Klein, D. T. Reindl, et al., Impact of HRSG characteristics on open volumetric receiver CSP plant performance, *Solar Energy* 127 (2016) 159–174.
- [33] A. S. Hassan, M. A. Darwish, Performance of thermal vapor compression, *Desalination* 335 (1) (2014) 41–46.
- [34] H. El-Dessouky, H. Ettouney, I. Alatiqi, G. Al-Nuwaibit, Evaluation of steam jet ejectors, *Chemical Engineering and Processing: Process Intensification* 41 (6) (2002) 551–561.
- [35] A. B. Amer, Development and optimization of ME-TVC desalination system, *Desalination* 249 (3) (2009) 1315–1331.
- [36] S. Shen, S. Zhou, Y. Yang, L. Yang, X. Liu, Study of steam parameters on the performance of a TVC-MED desalination plant, *Desalination and Water Treatment* 33 (1-3) (2011) 300–308.
- [37] I. J. Esfahani, A. Ataei, V. Shetty, T. Oh, J. H. Park, C. Yoo, Modeling and genetic algorithm-based multi-objective optimization of the MED-TVC desalination system, *Desalination* 292 (2012) 87–104.

- [38] S. M. Alelyani, N. W. Fette, E. B. Stechel, P. Doron, P. E. Phelan, Techno-economic analysis of combined ammonia-water absorption refrigeration and desalination, *Energy Conversion and Management* 143 (2017) 493–504.
- [39] J. D. DiBattista, J. Howard Choat, M. R. Gaither, J.-P. A. Hobbs, D. F. Lozano-Cortés, R. F. Myers, G. Paulay, L. A. Rocha, R. J. Toonen, M. W. Westneat, et al., On the origin of endemic species in the Red Sea, *Journal of Biogeography* 43 (1) (2016) 13–30.
- [40] D. E. Raitsos, I. Hoteit, P. K. Prihartato, T. Chronis, G. Triantafyllou, Y. Abualnaja, Abrupt warming of the Red Sea, *Geophysical Research Letters* 38 (14) (2011) 1–5.
- [41] O. Redlich, J. N. Kwong, On the thermodynamics of solutions. V. An equation of state. Fugacities of gaseous solutions., *Chemical reviews* 44 (1) (1949) 233–244.
- [42] C. Luo, N. Zhang, N. Lior, H. Lin, Proposal and analysis of a dual-purpose system integrating a chemically recuperated gas turbine cycle with thermal seawater desalination, *Energy* 36 (6) (2011) 3791–3803.
- [43] G. Xiao, T. Yang, H. Liu, D. Ni, M. L. Ferrari, M. Li, Z. Luo, K. Cen, M. Ni, Recuperators for micro gas turbines: A review, *Applied Energy* 197 (2017) 83–99.
- [44] A. Alkaiasi, R. Mossad, A. Sharifian-Barforoush, A review of the water desalination systems integrated with renewable energy, *Energy Procedia* 110 (2017) 268–274.